

Estimating Action Potential Thresholds From Neuronal Time-Series: New Metrics and Evaluation of Methodologies

Murat Sekerli, *Student Member, IEEE*, Christopher A. Del Negro, Robert H. Lee, and Robert J. Butera*, *Senior Member, IEEE*

Abstract—The estimation of action potential thresholds is a subjective process, which we quantified by surveying experienced electrophysiologists via a software application that allowed them to select action potential thresholds from several presented neuronal time series. Independent of this survey, we derived two nonparametric techniques for automating the detection of an action potential threshold from the time-series of intracellular recordings. Both methods start with a phase-space representation of the action potential (dV/dt versus V). Method I detects the maximum slope in the phase space, while Method II detects the maximum second derivative in the phase space. These two methods, as well as five additional methods in the literature, were tested on three data sets representing a variety of action potential shapes, the same three datasets that were used in the electrophysiologist survey. The database of user responses was used to provide an external benchmark against which to statistically evaluate all seven methods. Method II, as well as the curvature-based Methods VI and VII, provided the best results tracking both absolute and relative changes in threshold versus the other nonparametric methods (peak of second and third time derivatives). The one parametric method evaluated, detection of threshold crossing of the first temporal derivative, performed comparably to these methods, provided that an appropriate threshold was chosen. We conclude that Methods II, VI, and VII were the best methods evaluated due to their performance across a wide range of action potential shapes and the fact that they are nonparametric. Our user database of responses may be useful to other investigators interested in developing additional methods in that it quantifies what has often been a subjective estimate.

Index Terms—Action potential threshold, neuron, time series analysis.

Manuscript received September 4, 2003; revised January 16, 2004. The work of R. Butera was supported by the National Science Foundation (NSF) under Grant DBI-9987074 and Grant IBN-0131612 and by the National Institutes of Health (NIH) under Grant NS046851. The work of R. Lee was supported by the NIH under Grant NS046851. *Asterisk indicates corresponding author.*

M. Sekerli is with the Laboratory for Neuroengineering and the School of Electrical and Computer Engineering, Georgia Institute of Technology, Atlanta, GA 30332-0250 USA.

C. A. Del Negro was with the Feldman Laboratory, University of California, Los Angeles, CA 90095-1361 USA. He is now with the Department of Applied Sciences, College of William and Mary, Williamsburg, VA 23187-8795 USA.

R. H. Lee is with the Laboratory for Neuroengineering at Georgia Institute of Technology and the Wallace H. Coulter Department of Biomedical Engineering, Georgia Tech/Emory University, Atlanta, GA 30332-0250/30322 USA.

*R. J. Butera is with the Laboratory for Neuroengineering at Georgia Institute of Technology, the Wallace H. Coulter Department of Biomedical Engineering, Georgia Tech/Emory University and the School of Electrical and Computer Engineering, Georgia Institute of Technology, Atlanta, GA 30332-0250 USA (e-mail: robert.butera@ece.gatech.edu).

Digital Object Identifier 10.1109/TBME.2004.827531

I. INTRODUCTION

THE ACTION potential threshold is a quantifiable feature often correlated with a neuron's propensity to fire an action potential. While the physiological meaning of a true and absolute voltage threshold may be subject to debate [1], [2], it is still useful to quantify, both in experimental data and computational models. Electrophysiologists often quantify this threshold in spontaneously active, as well as stimulated, cells (primarily neurons and cardiac myocytes). Quantification of the action potential threshold is also useful for developing integrate-and-fire and Hodgkin-Huxley-style models from experimental data. Given the subjectivity of estimating action potential thresholds, we developed a software application where users (experienced electrophysiologists) examined a set of intracellular recordings and selected the points where they identified action potential thresholds. Time axis flexibility was provided so that each researcher could use the time/voltage scale that he/she was most comfortable with. The pooled results of this survey were used as a benchmark to test quantitative methods for action potential threshold detection, including two new methods proposed in this paper.

Many quantitative definitions of the action potential threshold exist. One of the most common definitions is the point at which the first temporal derivative of the membrane voltage trace exceeds an *ad hoc* value (e.g., 50 V/s in [3]; 10 V/s in [4]–[6]). Other definitions used in the literature include the points corresponding to the maximum of the second temporal derivative [7] and the third temporal derivative [8], [9] of the membrane voltage traces. Two additional methods are proposed in [10]. These curvature-based methods define a threshold via either the point of inflection or the maximum curvature of the action potential waveform.

In this paper, we propose two additional definitions for action potential threshold, and from these definitions derive methodologies for automatically calculating these threshold values from experimental data. These methods are nonparametric. We applied these methods, as well as others from the literature, to three different intracellular voltage trajectories in response to current ramp inputs: *in vitro* snail neurons, *in vitro* mouse brainstem neurons, and *in vivo* cat spinal cord motoneurons. In all three cases, the response is a train of action potentials steadily increasing in firing frequency and change in action

potential shape. The accuracy of each of these methods was then assessed by a statistical comparison against the pooled results of the electrophysiologist survey data. The accuracy of each method in tracking both absolute and relative change in threshold was quantified.

II. EXPERIMENTAL AND NUMERICAL METHODS

Experimental methods: Intracellular recordings were made from three preparations, i.e., motoneurons from the pond snail *Helisoma Trivolvis*, spinal motoneurons from a cat, and medullary brainstem neurons from a mouse. All experimental procedures for *in vivo* cat recordings were fully approved by the Institutional Animal Care and Use Committees at both Georgia Tech and Emory University. Mouse experiments used neonatal C57BL/6 mice (P0-10) and the Office for the Protection of Research Subjects (University of California Animal Research Committee) approved all protocols. Refer to [11] and [12] for intracellular recording methods for mouse neurons and cat motoneurons, respectively.

The pond snail *Helisoma Trivolvis* was used for invertebrate recording, and is an albino strain descended from the stock of Dr. V. Rehder (Georgia State University, Atlanta, GA). The buccal ganglia were microdissected and pinned to a Sylgard lined petri dish and soaked in a 1% pronase solution for 4 min for easier electrode penetration of the connective tissue. Conventional intracellular recording techniques were used to inject current and record membrane potential (3M KAc; $R_e = 15 \text{ M}\Omega$) under current clamp. The ganglia were perfused initially with normal *Helisoma* saline (in mM: NaCl 51.3, KCl 1.7, MgCl_2 1.5, CaCl_2 4.1) with HEPES 5 (pH 7.3). In some cases, ganglia were perfused with a saline solution including 25 μM FMRFamide, which acts on interneurons in the ganglia to stop rhythmic motor pattern activity [13]. All chemicals were obtained from Sigma-Aldrich (St. Louis, MO), except for pronase, which was obtained from Roche Pharmaceuticals (Basel, Switzerland). Intracellular recordings were made from motoneuron B5. Current injection and voltage measurement were via an Axoclamp 2-B (Axon Instruments, Foster City, CA) controlled by a computer running Clampex 8.2 software. All data were acquired with 16-bit resolution with a Digidata 1322A data acquisition module (Axon Instruments).

For all three classes of cells, a slow linearly increasing ramp of current was injected into each cell to depolarize it and elicit action potentials. Instead of using an input of step and/or pulse current, a ramp was used, because action potential pattern changes with increasing magnitude of input current for all cells examined. The bridge balance technique was employed to measure the membrane potential correctly in the presence of time-varying current waveform. We refer to the snail, cat, and mouse data sets as data sets A, B, and C, respectively.

Data Acquisition and Preprocessing: Intracellular time series were sampled at 20 kHz with 16-bit precision. All data sets were smoothed by applying a low-pass filter. This data smoothing was done prior to implementing any of the methods evaluated in this study. All methods performed poorly without this operation, due to the noise amplification of numerical estimates of derivatives. Several low-pass filters were compared to minimize the distortion of the action potential shape, and we

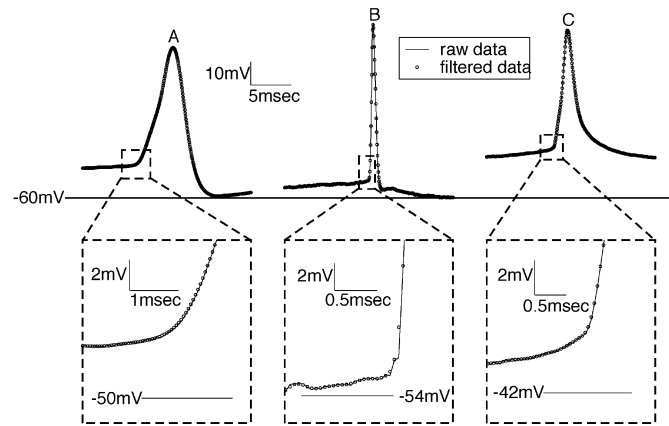


Fig. 1. Time course of action potential raw data (solid) with filtered data (o's): (A) snail data, (B) cat data, and (C) mouse data.

chose an eighth-order Bessel filter. The matched z-transform (MZT) [14], [15] was used to transform an analog Bessel filter to its digital counterpart. We performed zero phase digital filtering by processing the input data forward and then backward through the same filter [16], in order to eliminate frequency-dependent smearing of the action potential shape (phase distortion). For each data set, we used the lowest possible cutoff frequency that: 1) did not significantly distort the action potential waveform, particularly around the action potential threshold, where our estimates will be made and 2) allowed a reliable estimate of the third temporal derivative, which is particularly susceptible to noise. The cutoff frequencies used were 1250 Hz for the data set A and 2500 Hz for the data sets B and C. Fig. 1 illustrates the performance of this denoising operation; it shows the raw and filtered voltage trajectories for a single action potential of each data set. Filtering slightly reduced the peak of the action potentials, with an average decrease of 0.24, 1.46, and 0.15 mV in the action potential peaks for data sets A, B and C, respectively. However, the filter was quite effective at filtering baseline noise, without altering action potential shape considerably in the region of interest for threshold detection (see inset).

Derivative Estimates: Temporal derivatives were estimated with central difference techniques accurate to $O(\Delta t^4)$. The first, second, and third temporal derivatives at sample k were estimated as follows:

$$\begin{aligned} \frac{dV_k}{dt} &\approx \frac{x_{k-2} - 8x_{k-1} + 8x_{k+1} - x_{k+2}}{12\Delta t} \\ \frac{d^2V_k}{dt^2} &\approx \frac{-x_{k-2} + 16x_{k-1} - 30x_k + 16x_{k+1} - x_{k+2}}{12\Delta t^2} \\ \frac{d^3V_k}{dt^3} &\approx \frac{x_{k-3} - 8x_{k-2} + 13x_{k-1} - 13x_{k+1} + 8x_{k+2} - x_{k+3}}{8\Delta t^3} \end{aligned}$$

These estimations follow from Taylor series expansions and are more fully explained in most numerical analysis and mathematical reference texts [17].

Survey Data: Data sets A–C, which consist of a time-voltage trajectory in response to a steadily increasing ramp of injected current and include numerous action potentials, were incorporated into a user-interactive software program written in LabView (National Instruments). This program allows the user to examine each data set at adjustable time and voltage

scales and select the location of each action potential threshold. This software was distributed to several individuals ($N = 7$), all of whom were experienced with intracellular recording and current clamp techniques. After selecting the action potentials, the software program wrote the selected (t, V) data points to a file. These files were submitted via email to one of the coauthors, who assigned each user response an anonymous code number.

Our comparisons of the algorithms to the survey data use statistical measures including the mean and standard deviation of the researchers' estimates for each action potential threshold in each data set. The resulting measures are calculated as follows:

$$\mu_{v,i} = \frac{1}{N} \sum_{j=1}^N V_{th,i,j} \quad (1)$$

$$\sigma_{v,i} = \sqrt{\frac{1}{N-1} \sum_{j=1}^N (V_{th,i,j} - \mu_{v,i})^2} \quad (2)$$

where $\mu_{v,i}$ is the mean of the N responses for the i th action potential threshold of the survey data; $\sigma_{v,i}$ is the standard deviation of the i th action potential threshold of the survey data and $V_{th,i,j}$ is the i th threshold voltage estimated by the j th researcher. These calculations are performed for each action potential in each data set. All computations were performed with MATLAB (Mathworks, Natick, MA).

III. QUANTIFICATION OF THRESHOLD

Fig. 2(a) illustrates the time course of a typical action potential; Fig. 2(b) illustrates the same trajectory projected in an estimated $(dV)/(dt)$ versus V (V' versus V) phase space. Several investigators have found that the V' versus V phase space is useful for studying the dynamics of intracellular neuronal recordings [18]–[20]. We have found that for all types of data examined, the action potential threshold is visually discernable in the V' versus V space; thus, it is the focus of our analysis. While such a threshold is easily visualized, we wish to develop a precise definition that can be implemented by a mathematical algorithm.

We assume, for this analysis, that $V' \propto -I_M$, where I_M is the transmembrane ionic current. Thus, each action potential is typically reflected by a single clockwise trajectory winding in the V' versus V phase space [Fig. 2(b)], where the initial upward deflection represents the inward Na^+ current, during the depolarizing phase of the action potential, and the subsequent downward deflection represents the outward K^+ current, during the repolarizing phase of the action potential, followed by a return to rest.

The point in V' versus V where V' starts to increase noticeably is marked with a circle in Fig. 2(b) on the graph. That point is defined as the threshold and the corresponding voltage is defined as the threshold voltage V_{th} . Our derivations of both techniques for estimating V_{th} will refer to this diagram.

A. Method I—Maximum Slope

Method I assumes that the action potential threshold is the voltage where V' shows a maximal rate of change with respect

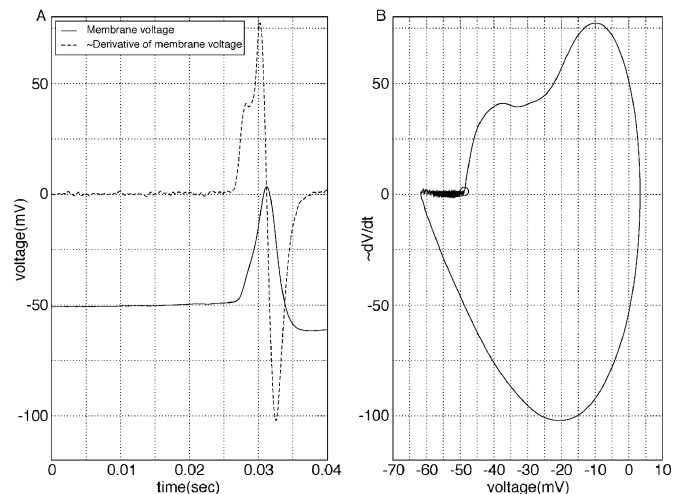


Fig. 2. (A) Time course of action potential (solid) and numerically estimated first derivative with respect to time (dashed). (B) V' versus V phase space projection of quantities in (A). V' values were linearly scaled for representational purposes. Circle in (B) denotes the region where V' starts to increase remarkably.

to V , i.e., the maximal slope of V' versus V . This assumption defines V_{th} as the voltage corresponding to a maximal increase in a change in inward current (proportional to I_{Na}) relative to V . Our definition of V_{th} utilizes the following definitions:

$$f = \frac{dV}{dt} = V' \quad (3)$$

$$g(t) = \frac{df}{dV} = \frac{df}{dt} \frac{dt}{dV} = \frac{\frac{df}{dt}}{\frac{dV}{dt}} = \frac{\frac{d^2V}{dt^2}}{\frac{dV}{dt}} = \frac{V''}{V'} \quad (4)$$

where V_{th} is the membrane potential where the maximum positive value of $g(t)$ occurs, within the region where $V' > 0$ for each action potential. Thus, the maximum value of $g(t)$ is the maximum slope of the V' versus V graph in Fig. 2(b).

B. Method II—Maximum Second Derivative in the Phase Space

Method II identifies for the point in the V' versus V the trajectory with the maximum second derivative with respect to voltage in the phase space (as opposed to slope); this is the point where the trajectory starts to make a strong departure from rest and represents the strong initiation of inward current. Our definition of V_{th} utilizes the following definitions:

$$\begin{aligned} h(t) &= \frac{d}{dV} \frac{df}{dV} = \frac{d}{dV} g = \frac{dg}{dV} = \frac{dg}{dt} \frac{dt}{dV} = \frac{\frac{dg}{dt}}{\frac{dV}{dt}} \\ &= \frac{\frac{V'''V' - (V'')^2}{(V')^2}}{V'} = \frac{V'''V' - (V'')^2}{(V')^3} \end{aligned} \quad (5)$$

where V_{th} is the membrane potential at the maximum positive value of $h(t)$, which occurs within the region where $V' > 0$, for each action potential. Thus, the maximum value of $h(t)$ is the maximum second derivative with respect to voltage in the region of the V' versus V phase plot of Fig. 2.

C. Methods III–V

Method III specifies the voltage threshold as the membrane potential corresponding to a positive crossing of a predetermined value of the first derivative of the membrane potential trajectory [3]–[6]. However, most investigators choose this threshold in an *ad hoc* manner, without reporting their rationale for their choice of dV/dt threshold. For comparison in this study, we chose a derivative threshold value that corresponded to the average dV/dt at the mean action potential threshold calculated from the survey data. While this choice is clearly biased by the very survey results we are using as a benchmark for all methods, this was intentionally done to choose a “best case” threshold. Therefore, when comparing Method III to other methods, we are relatively confident that this choice of threshold is the best case choice and alternative choices will not yield better performance from this method. In this paper, we consider the reliability of Method III as a function of the choice of threshold.

Method IV identifies the action potential threshold by the voltage corresponding to the maximum value of the second derivative of the membrane voltage [7]. Method V applies a similar approach but uses the temporal peak of the third derivative estimate [8], [9].

D. Methods VI and VII

Method VI locates the inflection point at the leading edge of the action potential. The inflection point is defined as the minimum of dV/dt . Method VII finds the point of the maximum curvature from [21]

$$K_p = V'' [1 + (V')^2]^{(-\frac{3}{2})}. \quad (6)$$

IV. RESULTS

Three different time series of action potential data were examined. Data set A consisted of action potentials from motoneuron B5 in the pond-snail *Helisoma Trivolvis*; this was chosen because of the slower time course of invertebrate neurons. Data set B used recordings of action potentials from *in vivo* spinal motoneurons of a cat; these neurons have the most rapid upstroke and were the noisiest of all three data sets. The last data set, C, was a recording of action potentials from medullary brainstem neurons of a mouse. Fig. 3 illustrates the initial portion of each of these three time series. Fig. 4 illustrates a close-up of the first action potential in each time series and includes the estimated action potential thresholds of Methods I–VII. The panels of both figures are labeled according to their corresponding data set. Left panels illustrate the time series, while the right panels illustrate the phase-space reconstruction.

To compare each method against the survey data, we calculated a hit rate (HR) for each data set and method. HR is defined as the percentage of the estimates in a given data set that fall within the mean \pm standard deviation of the survey data. We denote each estimated threshold by $V_{th,X,i}$: the threshold voltage of the i th action potential estimated by method X. A hit occurs when $V_{th,X,i}$ falls within the range $[\mu_{v,i} - \sigma_{v,i}, \mu_{v,i} + \sigma_{v,i}]$. Table I tabulates the HR for each method on each data set, along

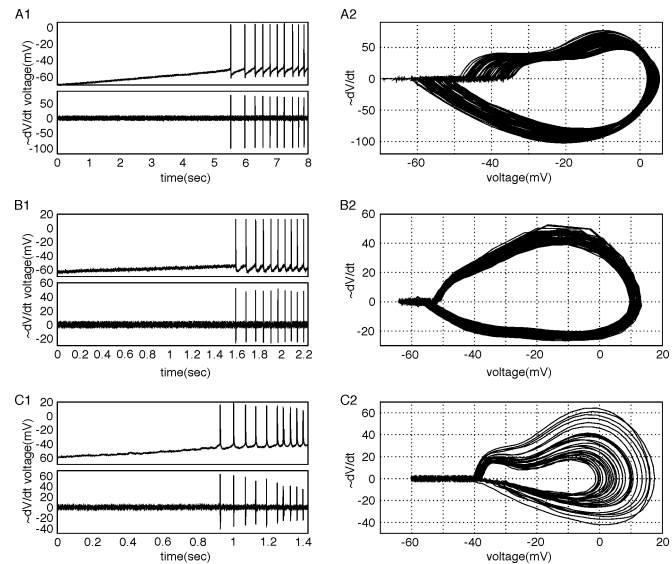


Fig. 3. Time course of membrane potential and first temporal derivative (A1/B1/C1) and phase-space projection (A2/B2/C2) for data sets A, B, and C. Absolute values in time axis have been shifted for consistent presentation.

with the mean-adjusted hit rate (MAHR), described below. By using the user data as a benchmark we assume that the estimates from seven researchers represent a global consensus on the values of the action potential thresholds. Given this assumption, the HR quantifies how successful each method is. Based on HR, Method III is the most successful followed by the methods VII, II, and VI. The success of particular methods was often data set dependent.

For each action potential in each data set, an error was calculated between the estimated threshold, $V_{th,X,i}$ for method X, and the corresponding survey threshold value $\mu_{v,i}$. As an example, for method I

$$e_{I,i} = V_{th,I,i} - \mu_{v,i} \quad (7)$$

where $e_{I,i}$ is the error in the estimate of the i th action potential threshold using method I. The mean (μ_e) and standard deviation (σ_e) of the errors ($e_{X,i}$) are summarized in Table II.

The mean error is an estimate of the general offset of each method. Averaged across the entire time series, most methods on most data sets had depolarized (positive) mean estimates from the survey estimates. For the data set A, the order of the methods in terms of increasing offset are VI, II, VII, III, I, V, and IV. For the data set B, the order is VI, VII, II, I, III, V, and IV; and for the data set C, the order is III, I, VII, II, V, VI, and IV. In general, the offset error is data set dependent.

In many cases, offset error is not important, because many experimentalists are only concerned with measuring changes in action potential threshold [5], [6], [9]. A metric with consistent offset error may still be very accurate in estimating changes in action potential threshold. Table II also tabulates the standard deviation of the error for each method on each data set, which provides a measure of how consistent or variable the error of each method is. For example, method III had the lowest variability in estimate error on all data sets.

To fairly assess how well each method can track changes in threshold (as opposed to absolute estimates), we recomputed

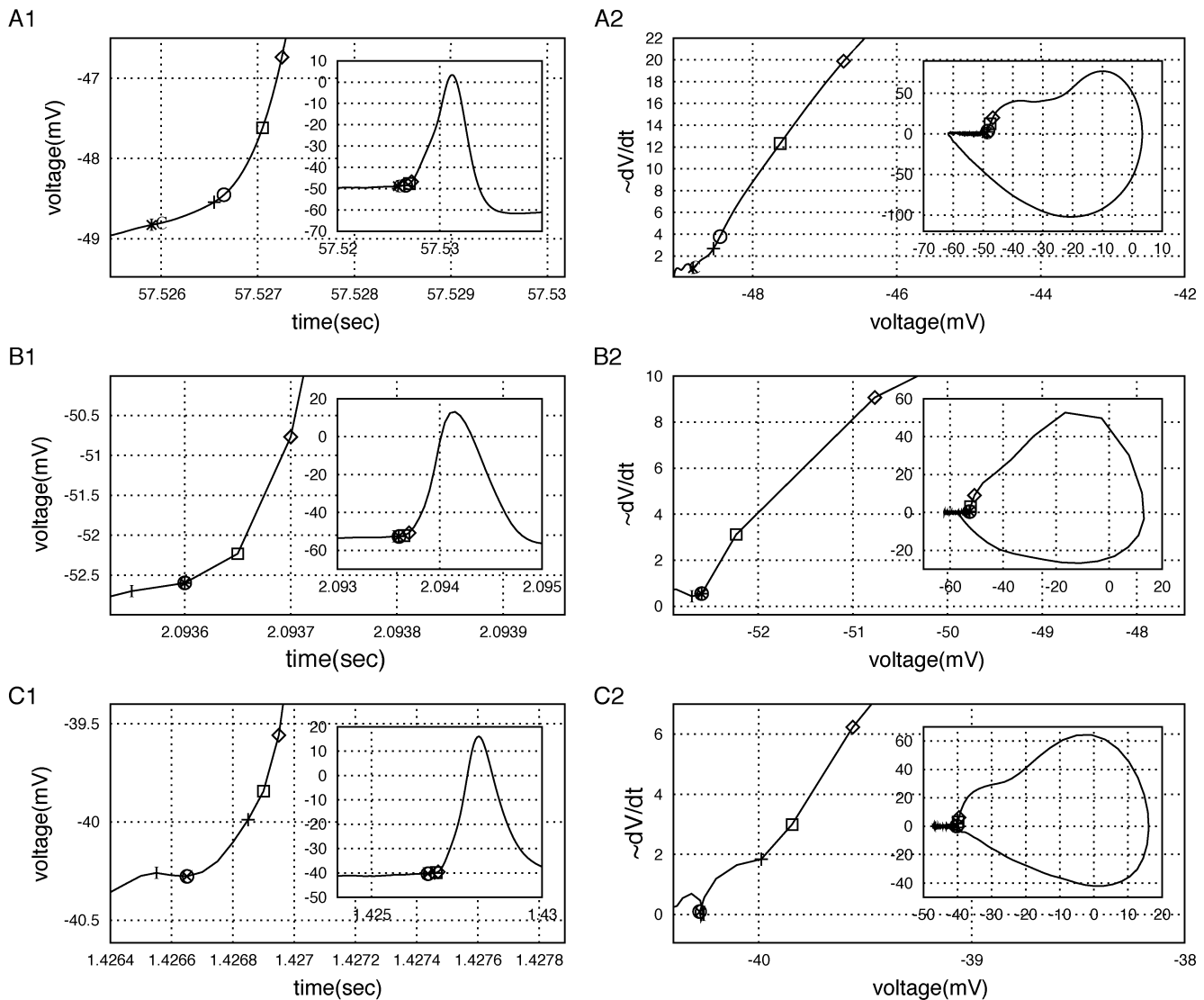


Fig. 4. First action potential from time series in Fig. 3. O's and X's represent estimated action potential threshold with Methods I and II, respectively. Plus, diamonds, and squares represent estimated action potential threshold with Methods III, IV, and V, respectively. I and C represent estimated action potential threshold with Methods VI and VII, respectively.

TABLE I
HIT RATES AND MEAN ADJUSTED HIT RATES

	A		B		C	
	HR (%)	MAHR (%)	HR (%)	MAHR (%)	HR (%)	MAHR (%)
I	72.7	90.9	94.4	95.8	53.6	71.4
II	98.5	98.5	100	100	67.9	82.1
III	100	98.5	91.5	100	100	96.4
IV	0	93.9	0	62.0	14.3	89.3
V	40.9	93.9	46.5	73.2	46.4	89.3
VI	98.5	98.5	100	100	53.6	96.4
VII	98.5	98.5	100	98.5	71.4	85.7

TABLE II
MEAN AND STANDARD DEVIATIONS OF ESTIMATION ERROR

	A		B		C	
	μ_e (mV)	σ_e (mV)	μ_e (mV)	σ_e (mV)	μ_e (mV)	σ_e (mV)
I	0.74	0.57	0.21	0.30	0.11	0.37
II	0.32	0.33	0.11	0.22	-0.25	0.25
III	0.45	0.24	0.31	0.20	0.05	0.17
IV	2.31	0.53	1.71	0.59	0.56	0.23
V	1.20	0.50	0.79	0.59	0.30	0.20
VI	0.27	0.30	0.04	0.20	-0.32	0.24
VII	0.37	0.35	0.09	0.24	-0.22	0.27

each estimate with a MAHR. All data sets with all methods were reanalyzed by taking all of the threshold estimates and adjusting them by the mean error for that data set and method, with the following:

$$V_{th,X,i,mae} = V_{th,X,i} - \mu_{e,X} \quad (8)$$

where “mae” stands for mean adjusted estimate, and $\mu_{e,X}$ is the μ_e from Table II with method X. Using this revised set of threshold estimates, the MAHR was the fraction of threshold estimates that lie inside the interval $[\mu_{v,i} - \sigma_{v,i}, \mu_{v,i} + \sigma_{v,i}]$. MAHR is included in Table I. Fig. 5 illustrates mean adjusted estimates for the first ten action potentials in the data set A.

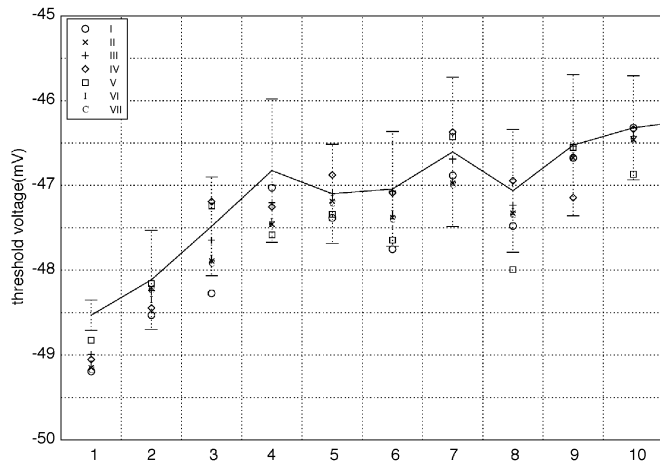


Fig. 5. Comparison of the methods' results for data set A with mean adjusted estimates. X axis is action potential number, Y axis is membrane potential. Line connects mean of estimates for each action potential, bars represent standard deviation of those estimates. Each point represents an estimate of a particular method; an estimate falling within the bar is a "hit." Legend mediates symbols used for each method.

Method III, which utilizes a threshold crossing detection of the first temporal derivative, was biased in that we utilized *a priori* knowledge of the user database results to set a threshold. This was done to identify a "best case" performance of this method. As the results show, this method performs quite well and was among the best tested. However, in practice, this threshold is estimated in an *ad hoc* manner so we studied how the HR changed as a function of threshold choice. These results, for all three data sets, are illustrated in Fig. 6. Relatively similar results are obtained if the MAHR is plotted instead (not shown).

The methodology presented here may have applicability beyond the analysis of experimental data. It may be possible to apply these methods to computational models to analytically determine action potential threshold, assuming that partial derivatives, with respect to membrane potential, can be computed. A relatively simple computational model that can be used to compare the performance of the methods presented here is the Morris–Lecar model [22]–[24]. While this model is relatively simplistic (simpler than the Hodgkin–Huxley model), it provides an ideal model against which to test these threshold identification methods since the threshold can be mathematically determined. In the model's excitable parameter regime, there exists a stable manifold in its phase plane that acts as a threshold barrier, which we can use as an absolute voltage threshold to compare to the results of the methods. This stable manifold can be numerically computed using the software package XPPAUTO [25] and is a function of the states of membrane voltage V and the recovery variable w . Integrating from an initial state near the threshold, Methods II and VI provide the closest estimates to the known threshold of the model. Method II estimated a threshold of -19.71 mV (versus an actual threshold of -19.96 mV) and Method VI estimated a threshold of -19.85 mV (versus an actual threshold of -20.07 mV). The actual thresholds were determined by using the value of the state variable w at the proposed threshold

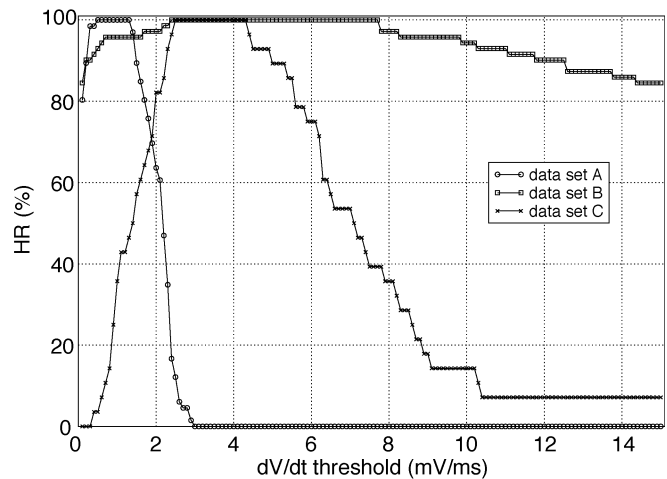


Fig. 6. Comparison of HR for different dV/dt thresholds. Quantized levels are the result of the finite number of action potentials in the data sets.

crossing and identifying the corresponding value of V (given w) that lies on the stable manifold.

V. DISCUSSION

The validity of our methods I and II, as well as the other methods we have compared our results to, is somewhat subjective. The subjectivity stems from the fact that there is no exact definition of the voltage threshold in the literature without considering the input current stimuli and/or spiking mode [2]. We attempted to deal with the subjectivity of estimating action potential thresholds by quantifying this via a user survey. These survey data were used as a benchmark for all seven methods; some of which enable both the reliable quantification of the subjective voltage threshold and the quantification of the changes in the voltage threshold.

All methods produced results within a few millivolts of each other. For data sets where the action potential threshold has a sharp onset, the methods perform comparably. However, Methods III, II, VII, and VI were among the best for all three data sets, while some methods excelled at one particular data set but not another. The second- and third-derivative methods (IV and V) performed poorly, while they had a MAHR approaching that of the other methods (even better for some cases), suggesting that they work well in detecting the changes in the threshold.

Fig. 6 illustrates that if using Method III, choice of threshold is critically important. In practice, this value is based on an *ad hoc* estimate by an experimentalist, and there is no independent set of data (like our database) available to evaluate the validity of this choice. We were unable to determine a reliable heuristic for selecting this value based on features of the data, such as defining the threshold as a fraction of the peak dV/dt value encountered during the action potential.

One characteristic of the data worth mentioning is the sampling frequency. In order to be able to acquire satisfactory estimates for the first or higher order derivative estimates, the sampling frequency must be high. We found this through trial and error when performing this study, and this is why we chose

a sampling rate of 20 kHz, typically much higher than what is commonly used to sample intracellular recordings. However, the disadvantage of choosing a high sampling frequency is the increase in baseline noise, which compromises the very derivative estimates that we are trying to quantify. Another important characteristic of the data is the bandwidth of the action potentials that also affects the determination of the sampling rate. The sampling rate chosen in this study is larger than the bandwidth of the action potentials, thus guaranteeing the satisfactory representation of the action potentials.

The shape of the trajectory itself may sometimes fool automated methods. For example, consider the phase-space projections of data set A (Fig. 3). A plot of dV/dt for data set A has an increase followed by an almost flat characteristic followed by a final increase (second curvature) to the peak of dV/dt as we increase V on the x axis. When an algorithm is developed in order to locate the thresholds with the methods, careful attention must be given to the second curvature. Besides considering the points for which $V' > 0$, we must also assign an upper boundary for V' in order to avoid possible ambiguous threshold results from the second curvature. The upper V' boundary may be around the numerical value 8–9 in the scaled V' axis in Fig. 3. The data set C has even more interesting features. For some action potentials, V' versus V graph has local minima as the membrane voltage depolarizes. The upper V' boundary for C may be around the numerical value 6–7 in the scaled V' axis in Fig. 3. In the implementation of Methods I and II, it is good practice to also assign a lower boundary for V' and identify the maximum of g and h in this closed region of $[V'_{\text{lower boundary}}, V'_{\text{upper boundary}}]$. The lower V' boundary is the first point in the phase space where V' starts to increase with respect to V and never decreases until V' reaches $V'_{\text{upper boundary}}$. The utilization of the lower boundary for V' is dataset dependent similar to the usage of upper boundary for V' .

Methods I and II introduced in this study differ from the methods VI and VII [10] in that the derivatives are defined with respect to voltage (in the phase space), not time. The phase space derivatives are more intuitive in representing the changes in the membrane current with respect to the membrane voltage.

In summary, we believe that Method II proposed in this paper, and the previously proposed Method VI, are viable nonparametric methods that reliably estimate action potential thresholds across various action potential data shapes. We arrived at this conclusion by quantifying the human subjectivity of action potential threshold identification and using the resulting pooled statistics as a benchmark against which to evaluate different techniques. The raw waveforms and the user response data are freely available to others and may be useful as a benchmark for other techniques estimating action potential threshold. The user data set can be accessed at the URL: <http://www.neuro.gatech.edu/groups/butera/sekerli04/>.

ACKNOWLEDGMENT

The authors would like to thank J. DiGiovanni (now with National Instruments, Austin, TX), who wrote the LabView software for the action potential survey. They wish to thank members of the Calabrese Lab at Emory University and the

Laboratory for Neuroengineering at the Georgia Institute of Technology, who participated in the survey. They also would like to thank the reviewers for their comments which significantly improved the content of this manuscript.

REFERENCES

- [1] C. Koch, O. Bernander, and R. J. Douglas, "Do neurons have a voltage or current threshold for action potential initiation?," *J. Comput. Neurosci.*, vol. 2, pp. 63–82, 1995.
- [2] L. J. Borg-Graham, "Interpretations of data and mechanisms for hippocampal pyramidal cell models," in *Cerebral Cortex, Volume 13: Models of Cortical Circuitry*, E. G. Jones and P. S. Ulinski, Eds. New York: Plenum, 1997.
- [3] P. Andersen, J. Storm, and H. V. Wheal, "Thresholds of action potentials evoked by synapses on the dendrites of pyramidal cells in the rat hippocampus *in vitro*," *J. Physiol. (London)*, vol. 383, pp. 509–526, 1986.
- [4] R. M. Brownstone, L. M. Jordan, D. Kriellaars, B. R. Noga, and S. J. Shefchyk, "On the regulation of repetitive firing in lumbar motoneurons during fictive locomotion in the cat," *Exp. Brain Res.*, vol. 90, pp. 441–445, 1992.
- [5] S. Krawitz, B. Fedirchuk, Y. Dai, L. M. Jordan, and D. A. McCrea, "State-dependent hyperpolarization of voltage threshold enhances motoneurone excitability during fictive locomotion in the cat," *J. Physiol. (London)*, vol. 532, pp. 271–281, 2001.
- [6] Y. Dai, K. E. Jones, B. Fedirchuk, D. A. McCrea, and L. M. Jordan, "A modeling study of locomotion-induced hyperpolarization of voltage threshold in cat lumbar motoneurons," *J. Physiol. (London)*, vol. 544, pp. 521–536, 2002.
- [7] Z. F. Mainen, J. Joerges, J. R. Huguenard, and T. J. Sejnowski, "A model of spike initiation in neocortical pyramidal neurons," *Neuron*, vol. 15, pp. 1427–1439, 1995.
- [8] J. T. Porter, C. K. Johnson, and A. Agmon, "Diverse types of interneurons generate thalamus-evoked feedforward inhibition in the mouse barrel cortex," *J. Neurosci.*, vol. 21, no. 8, pp. 2699–2710, 2001.
- [9] D. A. Henze and G. Buzsaki, "Action potential threshold of hippocampal pyramidal cells *in vivo* is increased by recent spiking activity," *Neurosci.*, vol. 105, pp. 121–130, 2001.
- [10] A. V. Rossokhin and Y. Z. Saakyan, "Study of the dependence of the generation threshold of the nerve impulse on the mode of formation of the input signal on the basis of the hodgkin-huxley model," *Biophys.*, vol. 37, no. 6, pp. 969–973, 1992.
- [11] C. A. Del Negro, C. Morgado-Valle, and J. L. Feldman, "Respiratory rhythm: An emergent network property?," *Neuron*, vol. 34, pp. 821–830, 2002.
- [12] R. H. Lee and C. J. Heckman, "Bistability in spinal motoneurons *in vivo*: Systemic variations in firing patterns," *J. Neurophysiol.*, vol. 80, pp. 572–582, 1998.
- [13] A. D. Murphy, K. Lukowiak, and W. K. Stell, "Peptidergic modulation of patterned motor activity in identified neurons of *helisoma*," *Proc. Nat. Acad. Sci.*, vol. 82, no. 20, pp. 7140–7144, 1985.
- [14] J. G. Proakis and D. G. Manolakis, *Digital Signal Processing: Principles, Algorithms and Applications*. Englewood Cliffs, NJ: Prentice-Hall, 1995.
- [15] A. Antoniou, *Digital Filters: Analysis, Design and Applications*. New York: McGraw-Hill, 1993.
- [16] A. V. Oppenheim and R. W. Schaffer, *Discrete-Time Signal Processing*. Englewood Cliffs, NJ: Prentice-Hall, 1989.
- [17] W. H. Beyer, Ed., *Standard Mathematical Tables and Formulae*, 29th ed. Boca Raton, FL: CRC, 1991.
- [18] R. Guttman, S. Lewis, and J. Rinzel, "Control of repetitive firing in squid axon membrane as a model for a neurone oscillator," *J. Physiol. (London)*, vol. 305, pp. 377–395, 1980.
- [19] R. J. Butera, J. W. Clark, C. C. Canavier, D. A. Baxter, and J. H. Byrne, "Analysis of the effects of modulatory agents on a modeled bursting neuron: Dynamic interactions between voltage and calcium dependent systems," *J. Comput. Neurosci.*, vol. 2, no. 1, pp. 19–44, 1995.
- [20] J. F. Fohlmeister and R. F. Miller, "Mechanisms by which cell geometry controls repetitive impulse firing in retinal ganglion cells," *J. Neurophysiol.*, vol. 78, pp. 1948–1964, 1997.
- [21] S. I. Grossman, *Calculus*. New York: Academic, 1981.
- [22] C. Morris and H. Lecar, "Voltage oscillations in the barnacle giant muscle fiber," *Biophys. J.*, vol. 35, pp. 193–213, 1981.
- [23] B. Gutkin, G. B. Ermentrout, and M. Rudolph, "Spike generating dynamics and the conditions for spike-time precision in cortical neurons," *J. Comput. Neurosci.*, vol. 15, pp. 91–103, 2003.

- [24] J. Rinzel and B. Ermentrout, "Analysis of neural excitability and oscillations," in *Methods in Neuronal Modeling: From Synapses to Networks*, C. Koch and I. Segev, Eds. Cambridge, MA: MIT Press, 1989, pp. 135–171.
- [25] B. Ermentrout, *Simulating, Analyzing, and Animating Dynamical Systems: A Guide to XPPAUT for Researchers and Students*. Philadelphia, PA: Soc. Industrial Applied Math., 2002.



Murat Sekerli (S'98) received the B.S. degree in electrical and electronics engineering from Middle East Technical University, Ankara, Turkey, in 2001 and the M.S. degree in electrical and computer engineering from Georgia Institute of Technology, Atlanta, in 2003. Currently, he is pursuing the Ph.D. degree at the School of Electrical and Computer Engineering, Georgia Institute of Technology.

His research interests include biologically inspired control, oscillation mechanisms in both electrical and neuronal circuits, and biomedical signal processing.



Christopher A. Del Negro received the B.A. degree in kinesiology from Occidental College, Los Angeles, CA, in 1992 and the Ph.D. degree in physiological sciences from the University of California, Los Angeles (UCLA), in 1998.

From 1998 to 2001, he worked for the Cellular and Systems Neurobiology Laboratory at the National Institutes of Neurological Disorders and Stroke (NINDS), at the National Institutes of Health, Bethesda, MD, where he studied neural mechanisms of respiratory rhythm generation. In 2001, he was

awarded a Parker B. Francis Fellowship to continue his investigations of respiratory rhythm generation at the Systems Neurobiology Laboratory at UCLA, in the Department of Neurobiology. He is currently an Assistant Professor of Applied Science at the College of William and Mary, Williamsburg, VA.



Robert H. Lee received the B.S. degree in chemical engineering from Purdue University, West Lafayette, IN, in 1989 and the M.S. and Ph.D. degrees in biomedical engineering from Northwestern University, Evanston, IL, in 1994 and 1998, respectively.

From 1989 to 1992, he worked for M.W. Kellogg Engineering and Construction as a process Engineer. After a two-year stint as a Postdoctoral Researcher in the Laboratory of Dr. C. J. Heckman studying the properties of motoneuron and neuromodulation, he received a research faculty position at Northwestern

University, Evanston, IL. Since 2001, he has been an Assistant Professor in the Department of Biomedical Engineering, Emory University, Atlanta, GA, where he continues to do research in the intracellular mechanisms underlying neuronal output. His research interests include neural control of movement, motoneuron physiology, cellular level neuronal computation, and developing neuronal computer models.



Robert J. Butera (S'88–M'91–SM'03) received the B.S. degree in electrical engineering from Georgia Institute of Technology, Atlanta, in 1991 and the MSEE and Ph.D. degrees from Rice University, Houston, TX, in 1994 and 1996, respectively.

From 1996 to 1999, he was a Postdoctoral Fellow at the National Institutes of Health, Bethesda, MD, in the Mathematical Research Branch (NIDDK) and Laboratory of Neural Control (NINDS). Since 1999, he has been with the School of Electrical and Computer Engineering and a member of the Laboratory for Neuroengineering at the Georgia Institute of Technology, where he is

currently an Associate Professor. His research interests include computational electrophysiology, mechanisms for stable central pattern generation underlying motor behaviors, the neural control of breathing, and applications of real-time computing to electrophysiological experiments.